Science Advances

AAAS

advances.sciencemag.org/cgi/content/full/1/10/e1500947/DC1

Supplementary Materials for

Superresolution microscopy reveals a dynamic picture of cell polarity maintenance during directional growth

Yuji Ishitsuka, Natasha Savage, Yiming Li, Anna Bergs, Nathalie Grün, Daria Kohler, Rebecca Donnelly, G. Ulrich Nienhaus, Reinhard Fischer, Norio Takeshita

Published 13 November 2015, *Sci. Adv.* **1**, e1500947 (2015)
DOI: 10.1126/sciadv.1500947

This PDF file includes:

Other Supplementary Material for this manuscript includes the following:
(available at advances.sciencemag.org/cgi/content/full/1/10/e1500947/DC1)

Movie S1 (.avi format). Dual-color wide-field fluorescence movie of mEosFP*thermo*-TeaR and GFP-MT in a growing filamentous fungus (Fig. 1D).
Movie S2 (.avi format). PALM movie of mEosFP*thermo*-TeaR prepared from the moving-window binning images shown in Fig. 4, F to H.

Materials and Methods

PALM Imaging. PALM images were acquired at room temperature on a modified inverted microscope (Axiovert 200, Zeiss) equipped with a high N.A. water immersion objective (C-Apochromat, 63x, N.A. 1.2, Zeiss). We employed three diode-pumped solid-state lasers, with wavelengths 561 nm (Cobolt Jive, Cobolt, Solna, Sweden), 473 nm (LSR473-200-T00, Laserlight, Berlin, Germany) and 405 nm (CLASII 405-50, Blue Sky Research, Milpitas, CA) for excitation and photoactivation of the fluorophores. The laser sources were combined via dichroic mirrors (AHF, Tübingen, Germany) and guided through an AOTF (AOTFnC-400.650, A-A, Opto-Electronic, Orsay Cedex, France) to control the laser intensities at the sample prior to coupling into a single mode fibre (OZ Optics, Ottawa, Ontario, Canada). Cells were incubated at 28 °C overnight in a chambered cover glass. The fluorescent proteins were converted from their green to their red emitting forms using low intensity (0 – 50 W/cm²) 405 nm light and excited by 561 nm simultaneous illumination (200 – 400 W/cm²). After passing through the excitation dichroic (z 405/473/561/635, AHF, Tübingen, Germany), fluorescence emission was filtered by a 607/50 band-pass filter (AHF, Tübingen, Germany) and recorded with a back-illuminated EMCCD camera (Ixon Ultra 897, Andor, Belfast, Northern Ireland) at 50 ms/frame time resolution unless stated otherwise.

All PALM data analyses were done using custom written analysis software, a-livePALM, running under the MATLAB R2010b (The Mathworks, USA) environment. The molecule identification thresholding parameter, *P value*, of 0.04 was used to identify molecules for further fitting. The software was run on a personal computer using an Intel(R) Core(TM) i7-2600 processor clocked at 3.40 GHz with 8.0 GB memory and a NVIDIA GeForce GTX 560Ti graphics card with 1.0 GB memory.

Further analyses of PALM data were done using custom written Matlab programs based on molecule coordinates extracted by the a-livePALM software. For cluster analysis, only molecules with localization precision better than 70 nm and more than 50 registered photons were used for analysis and rendering. Molecules localized within 100 nm in space and 50 ms in time were considered to be

identical and assigned to a weighted value of 1/F (F is number of frames in which a particular molecule can be detected)(*47*). All detected single molecule locations were binned into a two-dimensional histogram using the weighted value with a bin size of 10 nm per sub-pixel. Thus, the intensity of each pixel in the final reconstructed image represents the real density of molecules in this area. For each pixel, we computed the number of neighbouring molecules within 50 nm. Only pixels with more than 10 neighbouring molecules were considered as a cluster area. Each cluster is defined as 8-connected object from such a cluster area. Finally, the properties, such as area and number of molecules, of each cluster can be obtained from these individual objects. Moving window time lapse binning images were also processed by a custom written Matlab code.

To estimate the number of molecules, apart from the weighted value correction, we have applied no other corrections for the following three main reasons. First, there are mEosFP*thermo*-TeaR fusion proteins with a non-functional (non-emitting) fluorescent protein domain (which results in undercounting of proteins). Second, not all mEosFP*thermo* molecules within the cluster may have been photoconverted within the observation time at a given location, and TeaR clusters can also move away within that time period, which also results in undercounting. Third, photoconvertible fluorescent proteins show blinking, i.e., they may transiently go dark, so that fluorescent signals from the same molecule could have been counted more than once (which results in overcounting). Overcounting may at least partially be corrected by including a dark time compensation procedure. However, while such a strategy is suitable for fixed cell samples, where protein complexes remain in one location, this is clearly not the case for our live cell samples. The aberrations described here are expected to partially cancel each other and, therefore, our data analysis should yield a reliable estimate of the number of proteins in the clusters.

Widefield epifluorescence images using mEosFP*thermo*-TeaR and GFP-MT (Fig. 3A) were also acquired using the same microscope setup used for PALM imaging. The tip region of the cell was initially exposed to 405 nm laser light for 10 s to pre-convert a sufficient number of mEosFP*thermo*

molecules for regular epifluorescence imaging. This was followed by co-illumination with 561 nm and 405 nm light for imaging at 200 ms exposure time. Acquired images were processed by Fiji (*46*).

Simultaneous epifluorescence and PALM imaging was done by exciting the cell using the 405 nm, 473 nm and 561 nm lasers and by recording the green and the red channels separately using an Optosplit (Cairn Research Ltd, UK) unit attached to the EMCCD camera. Although the green state mEosFP*thermo*-TeaR fluorescence emission overlaps with the signal from GFP-MT because GFP is significantly more abundant than TeaR, the overall contribution to the image is negligible (Fig. 3A and fig. S2C).

Modeling

Modeling parameters were either set; 1) using measured data, 2) fit to resemble TeaR profiles (qualitative data) and/or 3) to reproduce the negative correlation between actin cable and MT fluorescence data (quantitative data).

The hypha was modeled as a cylindrical tube with a diameter of 2.3 μm (*13*), capped with a hemispherical tip. To simplify computation, the hyphal tip was flattened out, and the central 50 μm^2 of the membrane, centered at the hyphal tip, was used for simulation. Exocytic and endocytic zones were set based on experimental images of actin patches, visualized by GFP tagged AbpA (actin binding protein)(*33*). The inner and outer boundaries were measured to have diameters of 1.2 and 1.9 μm centered at the hemispherical tip, respectively (n = 10). Thus, the surface areas of two hemispherical caps (one with each measured diameter) were used to calculate the radii of the inner and outer circles to be used as endocytic boundaries. The exocytic zone was defined as the area within the endocytic zone. Sites of actin-mediated exocytosis were defined as sites containing actin within the exocytic zone, and chosen at random. Sites of basal exocytosis/endocytosis were defined as sites, chosen at random, within the exocytic/endocytic zone.

During the simulation, we assumed that the cell was growing (i.e., membrane addition at the tip was greater than membrane removal). All membranes and proteins moving out of the simulated field of view were discarded and were assumed that they would not return during our simulated time. Addition and removal of plasma membrane at the tip was modeled using the same computational framework as done previously (*9*).

At the plasma membrane, TeaR proteins form clusters via the positive feedback between TeaA, MTs and TeaR (*13, 20*). This positive feedback was approximated in the model by imposing TeaR self-attraction: Plasma membrane associated TeaR was attracted to other plasma membrane associated TeaR. Putting TeaR self-attraction into the model allowed for the possibility that all TeaR on the simulated membrane could accumulate on one membrane position. However, there will be a physical limit to how much TeaR can occupy an area of membrane. In the model 'overcrowding' is prevented by a spreading function that counteracts TeaR self-attraction. The equation to describe TeaR movement on the surface of the plasma membrane is,

$$\mathrm{TR}_{i,j}^{t+1} = \mathrm{TR}_{i,j}^{t} + D_a\,\mathrm{TR}_{i,j}^{t}\left[\left(\frac{\mathrm{TR}_{i-1,j}^{t}}{\sum_{m=j-1}^{j+1}\sum_{n=i-2}^{i}\mathrm{TR}_{n,m}^{t}}\right)+\left(\frac{\mathrm{TR}_{i,j+1}^{t}}{\sum_{m=j}^{j+2}\sum_{n=i-1}^{i+1}\mathrm{TR}_{n,m}^{t}}\right)+\left(\frac{\mathrm{TR}_{i+1,j}^{t}}{\sum_{m=j-1}^{j+1}\sum_{n=i}^{i+2}\mathrm{TR}_{n,m}^{t}}\right)+\left(\frac{\mathrm{TR}_{i,j-1}^{t}}{\sum_{m=j-2}^{j}\sum_{n=i-1}^{i+1}\mathrm{TR}_{n,m}^{t}}\right)-\left(\frac{\mathrm{TR}_{i-1,j}^{t}+\mathrm{TR}_{i,j+1}^{t}+\mathrm{TR}_{i+1,j}^{t}+\mathrm{TR}_{i,j-1}^{t}}{\sum_{m=j-1}^{j+1}\sum_{n=i-1}^{i+1}\mathrm{TR}_{n,m}^{t}}\right)\right]+D_s\left[\frac{\left(\mathrm{TR}_{i-1,j}^{t}\right)^2}{4}+\frac{\left(\mathrm{TR}_{i+1,j}^{t}\right)^2}{4}+\frac{\left(\mathrm{TR}_{i,j-1}^{t}\right)^2}{4}+\frac{\left(\mathrm{TR}_{i,j+1}^{t}\right)^2}{4}-\left(\mathrm{TR}_{i,j}^{t}\right)^2\right],$$

where TR_i^t denotes the concentration of TeaR at position i at time t, and D_a, D_s are the movement coefficients of self-attraction and spreading, respectively (fig. S4, A and B). The values of D_a and D_s were chosen to satisfy a qualitative fit (fig. S4C). If the spreading was fast or the self-attraction was weak, then TeaR clusters were lost. On the other hand, if the spreading was slow or self-attraction was strong, then fewer, dense TeaR clusters were formed, termed as overcrowding above. Modeling TeaR movement on the plasma membrane as simple diffusion, the random movement of TeaR with diffusion coefficient, D, resulted in a range of TeaR profiles (fig. S4D). However, none of them had

sustained TeaR clusters nor could they reproduce the movement of TeaR clusters away from the hyphal tip.

TeaR is a prenylated protein (*20*) and, therefore, was modeled as membrane bound, moving from internal membranes to the hyphal tip plasma membrane via exocytosis, and internalized via endocytosis. Vesicle size was set based on the experimental data. A simulated vesicle was modeled as a perfect sphere with a radius of 0.02 μm. Exocytic and endocytic vesicles were assumed to have the same size in the model (*30*), so the net number of vesicles per second (N_v) could be calculated using measured growth rates, with the assumptions that; 1) exocytic vesicles add the plasma membrane necessary for growth, and 2) endocytic vesicles remove plasma membrane causing shrinking. N_v = number of exocytic vesicles (N_{ex}) minus the number of endocytic vesicles (N_{en}) per second. The rate of endocytosis has previously been estimated to be 30% of the rate of exocytosis in mating yeast (*9*). Thus, the rates of exocytosis and endocytosis can be expressed as proportions of N_v, $N_{ex} = \frac{10}{7}N_v$, and $N_{en} = \frac{3}{7}N_v$.

As the simulated hyphal tip is a cylinder capped by a hemisphere, simulated growth was calculated by considering an increase in the length of the cylinder. This assumes that any plasma membrane added to the tip is instantly smoothed to retain its hemispherical shape. The surface area added to the cylinder per second (sa_c), given a growth rate of g μm/s, is $sa_c = \pi dg$, where d is the diameter of the cylinder.

The net number of vesicles added to the hyphal tip to obtain the measured growth rate is, $N_v = \frac{sa_c}{sa_v} = \frac{dg}{4r_v^2}$ per second, r_v is the radius of a vesicle. The measured growth rate fluctuated between 5 nm/s and 16.7 nm/s (n = 10). These values were used to calculate the maximum and minimum net number of vesicles per second, and hence the maximum and minimum vesicle trafficking rates. The actin cable hypothesis was modeled such that vesicle insertion was positively correlated with actin abundance. Vesicle trafficking rates were set using a linear relationship between actin abundance at the tip, and maximum and minimum vesicle trafficking rates (fig. S5A).

MT arrival rate and residence time at the hyphal tip were set using experimental data. We recorded an average of 5.8 MTs per minute reaching the hyphal tip (5.8 ±1.7, n=20), with an average of 8.1 s residence time at the tip (fig. S5B). These are comparable values with other analyses (*48, 49*).

The correlation between MTs and actin intensity was calculated to be –0.36, providing a qualitative measure of comparison between the real and model system. Correlation calculations are sensitive to both sampling and data set size. Therefore, when calculating the correlation between simulated MTs and actin abundance (Fig. 5A) the same sampling and data set size, as used to obtain the experimental value, were used. To take all simulated data into account, correlation coefficients were calculated using all sets of 70 consecutive points at 1 s intervals, for a 1 h simulation, this gave 3532 correlation coefficients (fig. S5C). Not all correlation coefficients calculated were statistically significant. Here we show correlation calculations between microtubule number and actin abundance because the spread of coefficients was large, unlike TeaR and growth correlation which had a much narrower set of values (data not shown). Only statistically significant correlation coefficients were considered and used the percentage of those that were negative (or positive) as the correlation measure. For the simulation shown in figure S4, 1741 correlation coefficients were statistically significant and, of those, 76% were negative (fig. S5D).

Vesicles inserted at the calculated rate can either be associated with TeaR or not. The percentage of inserted vesicles with TeaR was fitted using qualitative data. When TeaR was associated with all secretory vesicles the TeaR concentration profile formed a stable cap at the tip **Figure 5B** bottom. As the percentage of TeaR empty vesicles was increased the TeaR profile became more dynamic until TeaR puncta were ‘pushed’ down the hyphae by the empty vesicles (fig. S6A). The percentage of secretory vesicles containing TeaR was set to 25 %. The percentage was comparable to the number of TeaR in one cluster speculated by PALM and the number of vesicles per one exocytosis event calculated by the growth speed and frequency of MT reaching tip membrane.

Actin accumulation at the hyphal tip takes place downstream of membrane bound TeaR via a complex of proteins, which includes formin SepA (*20*). Complex formation and actin accumulation is inferred as a time delay in the model, thus actin nucleation takes place at past sites of TeaR. Furthermore, actin accumulation only occurs if past TeaR is above a set threshold. Setting a TeaR concentration threshold on actin accumulation is similar to using a Hill function with high Hill coefficient or, more accurately, a step function. Actin dynamics mirror that of TeaR above the set threshold, with a time delay. The system was not qualitatively or quantitatively sensitive to changes in threshold, apart from the extremes. Actin threshold did influence the correlation between TeaR abundance and growth rate (fig. S6B), an actin threshold of 5 μM was chosen.

Vesicles containing TeaR are delivered to the hyphal tip on MTs (Fig. 1, D and E, and Fig. 3A). The number of TeaR containing vesicles delivered on each simulated MT, per second, was decided using a qualitative fit to data (fig. S6D). With one TeaR containing vesicle per MT per second, the TeaR on the plasma membrane was sparse. Increasing the TeaR vesicle delivery rate led to hyphal tip TeaR saturation. A delivery rate of two TeaR containing vesicles per MT per second was chosen. At the hyphal tip, TeaR containing vesicles are stored awaiting insertion into the plasma membrane at either the basal rate or at the actin dependent rate. Vesicles without TeaR are also present at the hyphal tip and are inserted into the membrane in the same manner. The number of TeaR proteins on exocytic vesicles carrying TeaR was calculated to be 1 or 2. The simulated number of TeaR proteins per TeaR containing vesicle was chosen at random (either 1 or 2) and converted into TeaR concentration on insertion into the tip.

Membrane associated TeaR degraded at a fixed rate, the rate was fitted qualitatively to the data (fig. S6E). Stable TeaR resulted in TeaR rings centered at the hyphal tip, rings were not seen in the data. Decreased TeaR stability led to sparsely populated hyphal tips. A TeaR degradation rate of 0.2 per second was chosen.

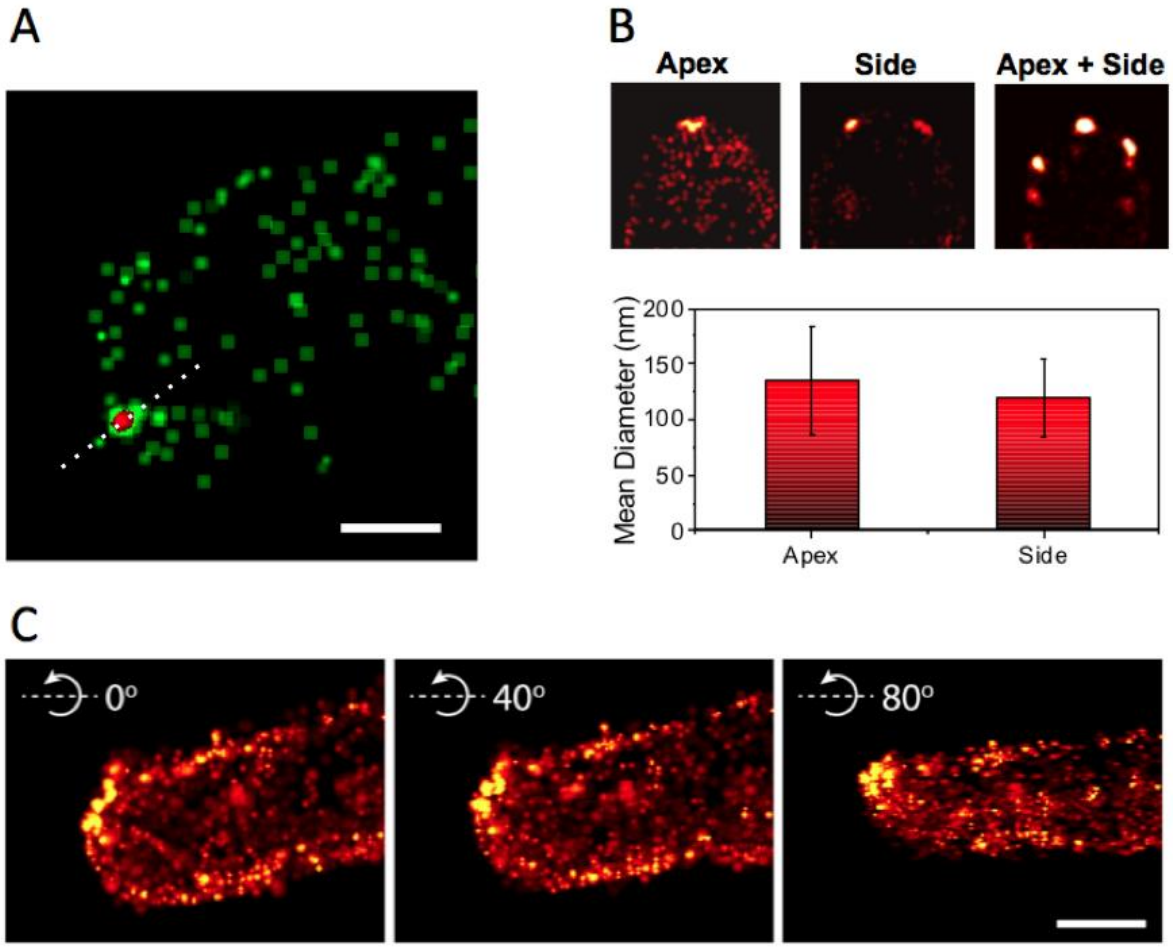

Fig. S1. The size quantifications and three-dimensional PALM imaging of TeaR clusters. (A) An example of a PALM image in Fig. 2B subjected to cluster analysis. The dotted line indicates the line used to obtain the intensity profiles shown in Fig. 2C. Identified molecules that had at least 5 molecules within 50 nm radius are colored in red (cluster); those with less neighbors are colored in green (non-cluster). From each of the identified clusters, the area and the number of molecules can be extracted. Not all clusters are spherical, but for ease of comparison, the diameter of a circle corresponding to the cluster area was calculated. The identified cluster sizes are greater than the localization accuracy of individual molecules and, therefore, closer to the real cluster dimensions. In order to estimate the number of secretory vesicles per measured cluster size, volumes of the cluster and the secretory vesicle were calculated from the fitted cluster diameter (118 ± 71 nm) and an estimated vesicle diameter of 40 nm. At least 50% of the cluster volume was assumed to be available to be filled by secretory vesicles (*50*). The scale bar is 500 nm. (B) The sizes of TeaR clusters at the apex and on the side near the apex did not differ significantly. (C) Three different projections (0°, 40° and 80°) of a 3D PALM image stack reconstructed from 10,000 frames within 300 s. From a perspective equivalent to the one of conventional 2D PALM (left), a single, elongated cluster would be identified near the tip. This feature, however, actually consists of four individual clusters, as is evident from the view at +80° (right).

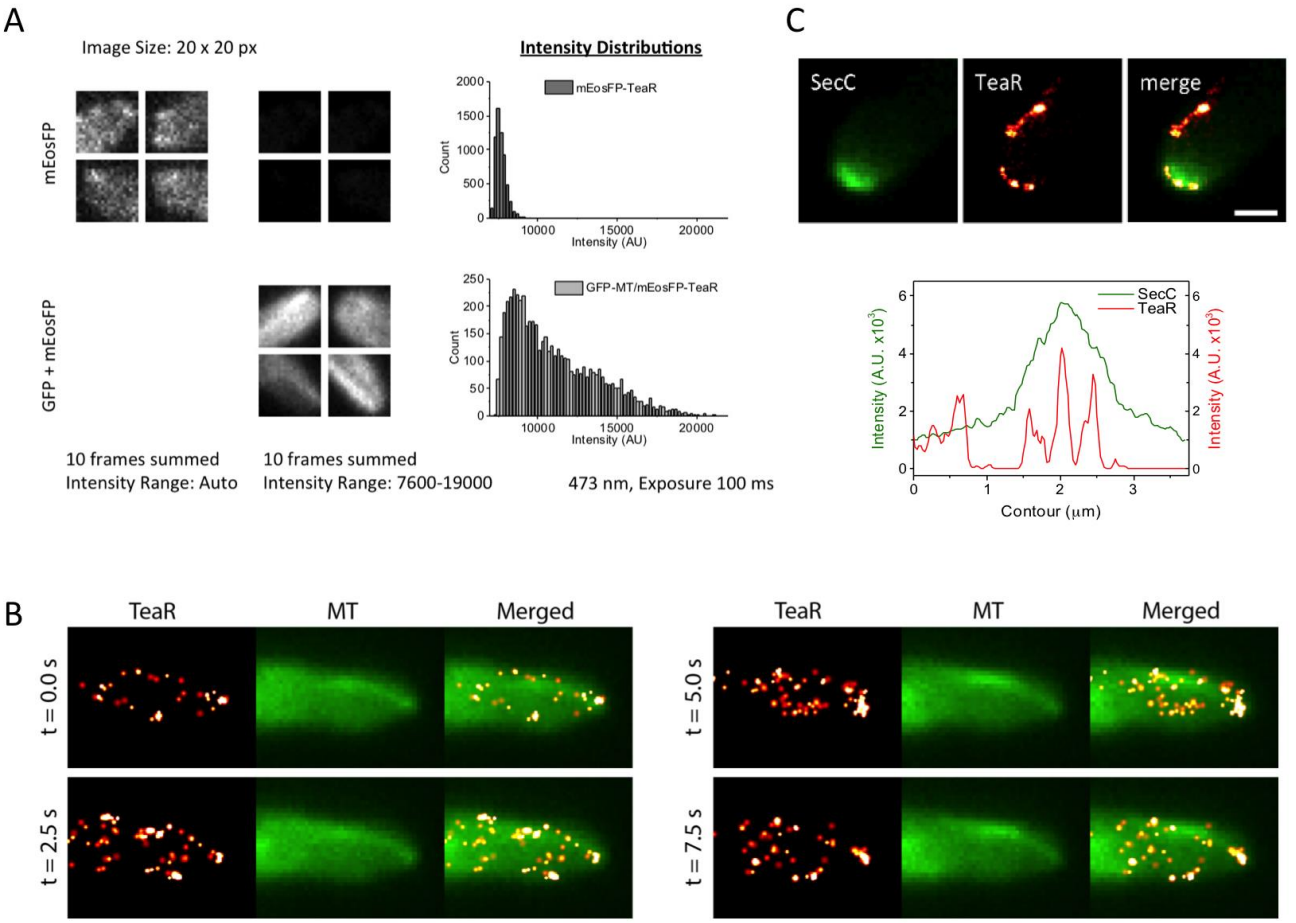

Fig. S2. **Simultaneous epifluorescence and PALM imaging.** (A) Intensity comparison between mEosFP*thermo*-TeaR (green state) and GFP-MT. In order to simultaneously image GFP and mEosFP*thermo* in our dual-channel fluorescence microscope, it is important that the GFP signal is much stronger than that of mEosFP*thermo* (green state) because mEosFP*thermo*'s green state spectrally overlaps with GFP. Four sample images of *A. nidulans* co-expressing mEosFP*thermo*-TeaR and GFP-MT are shown. Samples were excited at 473 nm and fluorescence signals were collected using an appropriate bandpass filter for the GFP channel. In all four examples, a TeaR signal is present (left top images) but the fluorescence intensity from MTs is several-fold higher than the one from mEosFP*thermo* (histograms on the right). Tubulin proteins, in general, are present inside cells at a much higher concentration than TeaR. When the intensity range of the images is adjusted for the analysis (middle column images), only the MT signal is visible. (B) Time-lapse fluorescence images of TeaR (PALM, 50 frames) and MTs (widefield). The elapsed time is given in seconds. Fewer numbers of frames were used to reconstruct PALM images to show TeaR molecules along the MTs more clearly. (C) Colocalization between SecC-GFP (widefield) and TeaR (PALM) and the corresponding intensity profiles of SecC and TeaR along the tip. Scale bar, 1 μm.

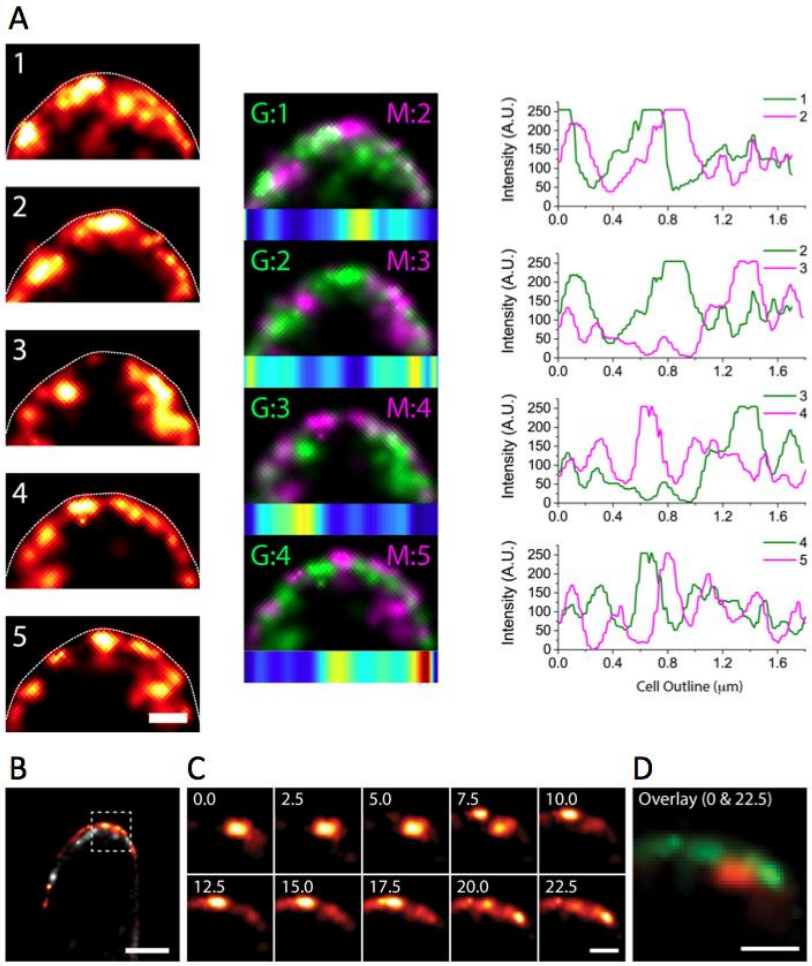

Fig. S3. **Distribution of TeaR cluster at different time scales.** (A)(left column) Series of five PALM images of hypha expressing mEosFP*thermo*-TeaR taken with 75 s time interval (1,500 frames each) used to prepare Fig. 4E. (middle column) The overlay of two successive PALM images (color and frame number indicated by numbers at top corners). Colocalized regions will appear in white with this combination of colors. The change of the cell profile along the y-axis between two subsequent images is shown as a color map below each overlaid images. (right column) Intensity profiles along the cell membrane from two successive image frames (corresponding to the middle column) were plotted. Both overlaid images and intensity profiles show that localization of TeaR clusters, especially the most concentrated clusters, do not overlay between successive frames. Scale bar, 300 nm. (C) Sequence of close-ups of the region marked by a square in (B), constructed by moving window binning (250 frames/image, with an increment 50 frames), so that one image corresponds to a time interval of 2.5 s. They show the appearance of a new cluster (white triangle, t = 5.0 s), a translational movement (t = 10.0 s) and a spreading of the signal along with a slight shift of the pattern. (D) Overlay of the first (red) and the last (green) frame from (C) shows a small shift of the pattern.

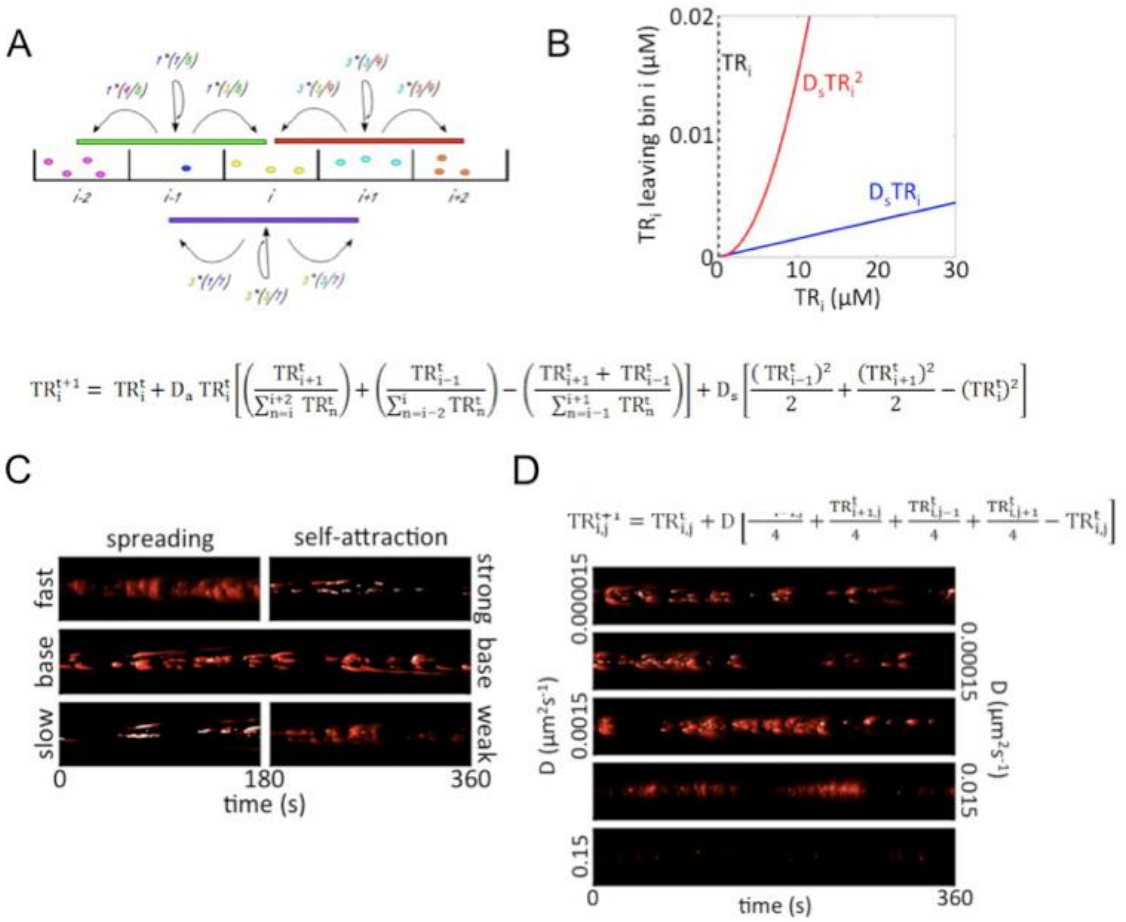

Fig. S4. Modeling of TeaR movement on the plasma membrane. (A) Diagrammatic example of TeaR self-attraction on a one-dimensional plasma membrane (equation shown below). Black segmented line shows five hypothetical membrane positions. Each position contains a TeaR concentration, shown as colored dots. Arrows give the direction of TeaR movement as a result of self-attraction. Concentration of TeaR moving in each direction shown by numbers on the arrows. Numbers are color coded to match TeaR concentrations in each position. The colored lines spanning three positions represent the sum of TeaR concentrations in the spanned positions, also color coded. (B) The spreading function is symmetrical, movement of TeaR out of position i depends only on TeaR concentration at position i. A linear equation for spreading (blue line) was unable to simultaneously allow puncta formation and reduce overcrowding. To mimic the idea of space limitation, the protein leaving position i was given a nonlinear relationship (red line) with the concentration at position i. This allowed puncta formation while limiting the TeaR concentration within puncta. (C) Qualitative fit of TeaR movement on the plasma membrane. Spreading movement D_s = {0.0015, 0.00015, 0.000015} $\mu m^2 s^{-1}$, for {fast, base set, slow}. Self-attraction D_a = {0.5,0.05,0.005} $\mu m^2 s^{-1}$, for {strong, bas, weak}. (D) Diffusive movement of TeaR on the plasma membrane. Intense dots are produced by the TeaR containing vesicles when inserted into the hyphal tip. The high TeaR concentration then diffuses over the membrane becoming more dilute.

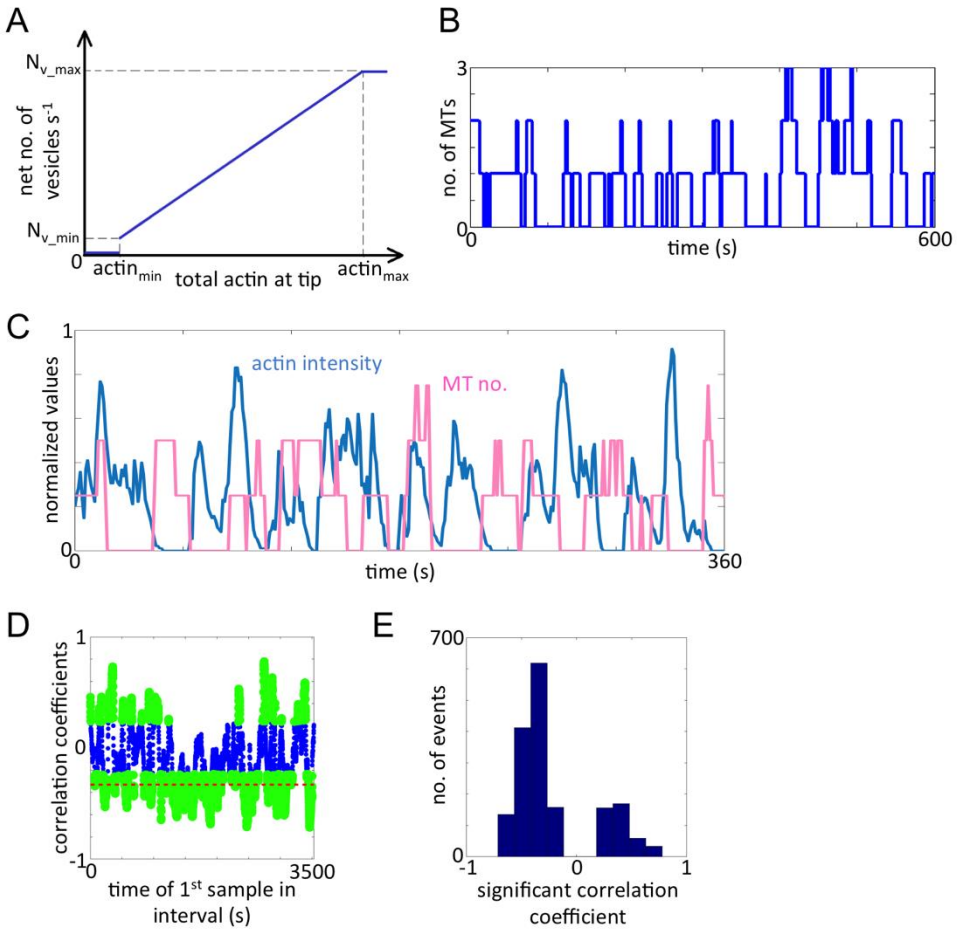

Fig. S5. Modeling of the actin and MT dynamics. (A) Illustration of the linear relationship between actin abundance at the hyphal tip and rate of vesicle insertion. $actin_{min}$ is the minimum amount of actin at the tip above zero, $actin_{max}$ is the maximum amount of actin. The values of $actin_{min}$ and $actin_{max}$ are dynamic and set during the simulation. (B) Time course of number of MTs at the tip over a 10 min period. (C) Simulated time course data for microtubule number and total actin intensity at the hyphal tip. (D) Correlation between actin intensity and MT number (blue dots). Green dots show statistically significant correlation coefficients. Red dotted line indicates the correlation coefficient calculated using biological data. (E) Histogram showing the frequency of significant correlation coefficients (same data as in (D)). 76% of significant correlation coefficients are negative.

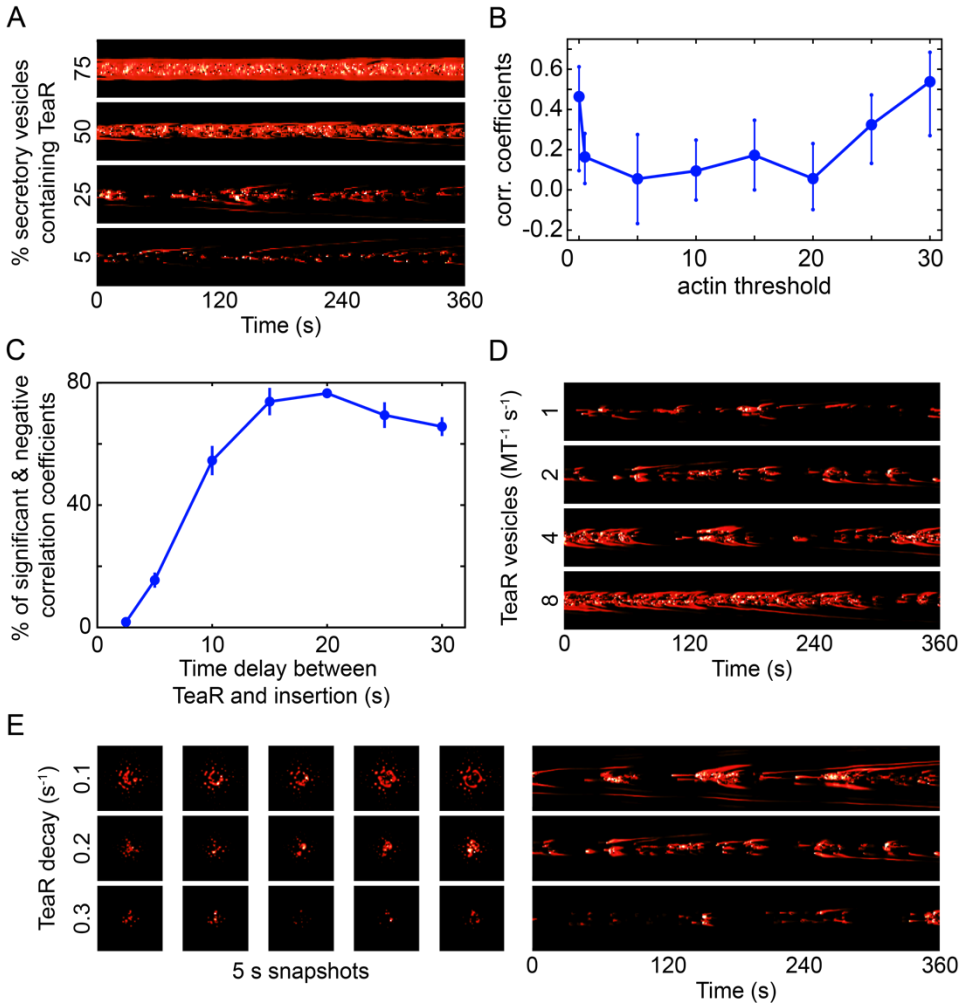

Fig. S6. Systematic evaluations of modeling parameters. (A) Qualitative fit for percentage of secretory vesicles containing TeaR. (B) Quantitative fit of actin threshold. Lines with dots show mean correlation coefficients taken from 5 one-hour simulations. Vertical lines show spread of correlation coefficients bound by maximum and minimum values. (C) Time delay between TeaR and actin mediated vesicle insertion, plotted against the percentage of negative correlation coefficients. Dots show the percentage of significant correlation coefficients with a negative value, averages taken from five one hour simulations. An average was calculated from each one hour simulation, these were then used to calculate the average values on the graph and standard the error bars. (D) Qualitative fit for the number of TeaR containing vesicles delivered to the tip per MT per second. (E) *left*. Qualitative fit for TeaR degradation. Snapshots of TeaR at the tip viewed from above. *right*. TeaR kymographs for each degradation rate.

Table S1: *A. nidulans* strains used in this study.

Strain	Genotype	Source
TN02A3	*pyrG89; argB2; pyroA4; [ΔnkuA::argB]*	(*51*)
LO2199	*pyrG89; argB2; ΔnkuA::argB; pyroA4; nicA2; [secC-gfp::pyroA]; [mcherry-sncA::pyrG]*	(*15*)
SNT127	*pyrG89; argB2; ΔnkuA::argB; pyroA4; [alcA(p)-mEosFPthermo-teaR::pyr-4]*	This study
SNT145	*pyrG89; argB2; ΔnkuA::argB; pyroA4; [teaR(p)-gfp-teaR::pyr-4] [bglA(p)-bglA-mcherry::pyroA]*	This study
SNT142	*pyrG89; argB2; ΔnkuA::argB; pyroA4; [pyroA]; [alcA(p)-mEosFPthermo-teaR::pyr-4] [alcA(p)-gfp-tubA::pyr-4]*	This study
SNT146	*pyrG89; argB2; ΔnkuA::argB; pyroA4; [alcA(p)-mEosFPthermo-teaR::pyr-4] [secC-gfp::pyroA]*	This study
SNT158	*pyrG89; ΔnkuA::argB?; pyroA4; [pyroA]; [alcA(p)-mEosFPthermo-teaR::pyr-4] [ΔteaA::argB]*	This study
SNT159	*pyrG89; ΔnkuA::argB?; [alcA(p)-mEosFPthermo-teaR::pyr-4] [ΔalpA::pyr-4]*	This study
SNT147	*pyrG89; argB2; ΔnkuA::argB; pyroA4; [alcA(p)-gfp-tpmA::pyr-4]*	This study
SARB5	*pyrG89; argB2; ΔnkuA::argB; pyroA4; [alcA(p)-gfp-tpmA::pyr-4] [alcA(p)-mcherry-tubA::pyroA]*	This study

Table S2. Parameters used in the hyphal tip simulations.

Unless otherwise stated, parameters for simulations are as above, referred to as the base set.

Name	value	unit	ref
vesicle diameter	40	nm	(*29*)
hyphal diameter	2.3	µm	**(***13***)**
min growth rate	5	$nm\ s^{-1}$	this study, data
max growth rate	16.7	$nm\ s^{-1}$	this study, data
microtubules reach tip	5.8	min^{-1}	this study, data
microtubule residence time	8.1	s	this study, data
Number of TeaR proteins per TeaR vesicle	1 or 2		this study, data
TeaR degradation	0.2	s^{-1}	this study, qualitative fit
self-attraction movement coefficient (D_a)	0.05	$\mu m^2\ s^{-1}$	this study, qualitative fit
spreading movement coefficient (D_s)	0.00015	$\mu m^2\ s^{-1}$	this study, qualitative fit
TeaR containing vesicle delivery rate	2	$MT^{-1}\ s^{-1}$	this study, qualitative fit
percentage of secretory vesicles containing TeaR	25		this study, qualitative & quantitative fit
TeaR threshold for actin accumulation	5	µM	this study, qualitative & quantitative fit
actin accumulation delay	20	s	this study, quantitative fit

Movie legends

Movie S1. Dual-color wide-field fluorescence movie of mEosFP*thermo*-TeaR and GFP-MT in a growing filamentous fungus (Fig. 1D).

Movie S2. PALM movie of mEosFP*thermo*-TeaR prepared from the moving-window binning images shown in Fig. 4, F to H.